MRS Advances © 2018 Materials Research Society
DOI: 10.1557/adv.2018.453

Synthesis and Characterization of Co_3O_4-$Mn_xCo_{3-x}O_4$ Core-Shell Nanoparticles

Ning Bian[1], Robert A. Mayanovic[1] and Mourad Benamara[2]

[1]*Department of Physics, Astronomy & Materials Science, Missouri State University, Springfield, MO 65897, U.S.A.*

[2]*Institute for Nanoscience & Engineering, University of Arkansas, Fayetteville, AR 72071*

ABSTRACT

The mixed-valence oxide Co_3O_4 nanoparticles, having the normal spinel structure, possess large surface area, active-site surface adsorption properties, and fast ion diffusivities. Consequently, they are widely used in lithium-ion batteries, as well as for gas sensing and heterogeneous catalysis applications. In our research, we use a two-step method to synthesize Co_3O_4–based core-shell nanoparticles (CSNs). Cobalt oxide (Co_3O_4) nanoparticles were successfully synthesized using a wet synthesis method employing KOH and cobalt acetate. Manganese was incorporated into the Co_3O_4 structure to synthesize inverted Co_3O_4@$Mn_xCo_{3-x}O_4$ CSNs using a hydrothermal method. By adjustment of pH value, we obtained two different morphologies of CSNs, one resulting in pseudo-spherical and octahedron-shaped nanoparticles (PS type) whereas the second type predominantly have a nanoplate (NP type) morphology. X-ray diffraction (XRD), scanning electron microscopy (SEM), transmission electron microscopy (TEM), and x-ray photoelectron spectroscopy (XPS) have been performed in order to determine the morphological and structural properties of our CSNs, whereas the magnetic properties have been characterized using a superconducting quantum interference device (SQUID) magnetometer. XRD and TEM results show that the CSNs have the same spinel crystal structure throughout the core and shell with an average particle size of ~19.8 nm. Our Co_3O_4 nanoparticles, as measured prior to CSN formation, are shown to be antiferromagnetic (AFM) in nature as shown by the magnetization data. Our SQUID data indicate that the core-shell nanoparticles have both AFM (due to the Co_3O_4 core) and ferrimagnetic properties (of the shell) with a coercivity field of 300 Oe and 150 Oe at 5 K for the PS and NP samples, respectively. The magnetization vs temperature data show a spin order-disorder transition at ~33 K and a superparamagnetic blocking temperature of ~90 K for both batches.

INTRODUCTION

Core-shell nanoparticles (CSNs) have drawn much attentions due to their finite-size dependent magnetic properties and because of their technological applications[1,2]. Bimagnetic CSNs, which have distinct core and shell magnetic properties, are being

explored for magnetic devices, medicals and other applications[3]. The mixed-valence oxide Co_3O_4 nanoparticles, having the normal spinel structure, possess large surface area, active-site surface adsorption properties, and fast ion diffusivities. Consequently, they are widely used in lithium-ion batteries [4,5], as well as for gas sensing [6] and heterogeneous catalysis applications [7]. Co_3O_4 has an ordered structure in the normal spinel phase with Co^{2+} ions occupying tetrahedral sites whereas the Co^{3+} ions occupy octahedral sites, for which the magnetic moment is derived from the Co^{2+} ions whereas Co^{3+} ions are nonmagnetic [8]. Bulk Co_3O_4 is antiferromagnetic in nature with a Néel temperature of 40 K. The shape-dependent exchange bias properties of bimagnetic nanostructured materials have drawn much interest from the scientific community. Fan et al. have studied the magnetic properties of urchin-like $Co_3O_4/CoFe_2O_4$ nanocomposites and claim that the mismatched surface spin in the hetero-structured $Co_3O_4/CoFe_2O_4$ nanocomposites are greatly reduced[9]. Chen et al have shown that octahedral Co_3O_4 nanoparticles exhibit an antiferromagnetic phase transition at a Néel temperature of ~10 K and much of the Co^{3+} ions are in the high-spin state[10]. Teng et al studied face-raised Co_3O_4 nano-octahedral shaped nanomaterials and found that they have a higher remanence and saturation magnetization compared to normal Co_3O_4 octahedral nanomaterials[11]. It is still unclear as to how the exchange bias effect is dependent upon the geometry of Co_3O_4-based bimagnetic nanostructures. Herein we used our hydrothermal nanophase epitaxy (HNE) method [12,13] to prepare $Co_3O_4@Mn_xCo_{3-x}O_4$ inverted CSNs with two different morphologies for the first time, and addressed the question as to how the magnetic properties depend upon their shape. Our bimagnetic CSNs were characterized using X-ray diffraction (XRD), scanning electron microscopy (SEM), transmission electron microscopy (TEM) and a SQUID magnetometry.

EXPERIMENTAL

Co_3O_4 nanoparticles were synthesized using a soft chemical approach [14]. A quantity of 0.04 M cobalt acetate was mixed with 0.1M potassium hydroxide aqueous solution to be used as a precursor. Next, we used hydrochloric acid and potassium hydroxide to adjust the pH value of the precursor solution to make two batches: one with a pH value of 9.5 (PS precursor solution) and another with a pH value of 8.5 (NP precursor solution). Both solutions were stirred for 2 hours at room temperature. Next, the solutions were refluxed in a water bath at 100 °C for 4 hours. After centrifugation, the residue was rinsed thoroughly using 50% ethanol solutions, and allowed to dry at room temperature. The resulting dark grey PS and NP powders were calcined at 450 °C and 550 °C in air for 4 hours, respectively. For both samples, we obtained black powder. The possible chemical reactions that result in the formation of Co_3O_4 nanoparticles are shown below:

$$Co(CH_3COO)_2 + 2.5\,KOH \rightarrow CoO + 2\,CH_3COOK + H_2O$$

$$6CoO + O_2 \rightarrow 2\,Co_3O_4$$

The Co_3O_4 nanoparticles were subsequently used to synthesize Co_3O_4 based $Mn_xCo_{3-x}O_4$ inverted core-shell nanoparticles using our hydrothermal Nano phase epitaxy (HNE) method[3]. For each type of sample, 20 ml distilled water was deoxidized with dry nitrogen gas for 20 minutes at room temperature. Subsequently, 0.176 g of $MnCl_2$ were dissolved and sonicated in the aqueous solution for 10 minutes. Hydrochloric acid was used to control the pH value to a value of the $MnCl_2$ solution close to 3.5, which was subsequently mixed with 0.337 g of PS or NP Co_3O_4 nanoparticles. The nanoparticle-solution mixture was first sonicated 30 minutes at room temperature and then transferred to an autoclave, where it was hydrothermally treated at 200 °C for 30 hours. The

resulting core-shell nanoparticles (CSNs) residue was subsequently rinsed using distilled water several times, centrifuged and dried at room temperature overnight.

SAMPLE CHARACTERIZATION

X-ray diffraction (XRD) of the core-shell nanoparticles was using a Bruker D8 Discover x-ray diffraction instrument. The x-ray diffractometer is equipped with Cu-Kα radiation (wavelength 1.54 Å) source: The XRD data were collected covering a 2θ range from 10 to 90°. An FEI Quanta 200 scanning electron microscopy was used for SEM imaging and energy dispersive x-ray spectroscopy (SEM-EDS) of the CSN samples. High-resolution imaging (HRTEM) and morphological characterization of the CSNs was made using an FEI Titan 80-300 transmission electron microscopy with an operating voltage of 300 KeV at the University of Arkansas. Hysteresis loop and magnetization vs temperature measurements of the CSN samples were obtained using a Quantum Design SQUID MPMS/XL magnetometer. Statistical analysis of the nanoparticles was made using ImageJ in the conjunction with the TEM images. The x-ray photoemission spectroscopy measurements were made using a Versa Probe XPS at the University of Arkansas. The x-ray source is a monochromated K-alpha radiation from aluminium at 1486 eV where the pass energy used for surveys and high-resolution scans was set at 117.4 and 58.7 eV, respectively.

RESULTS AND DISCUSSION

Electron Microscopy Imaging

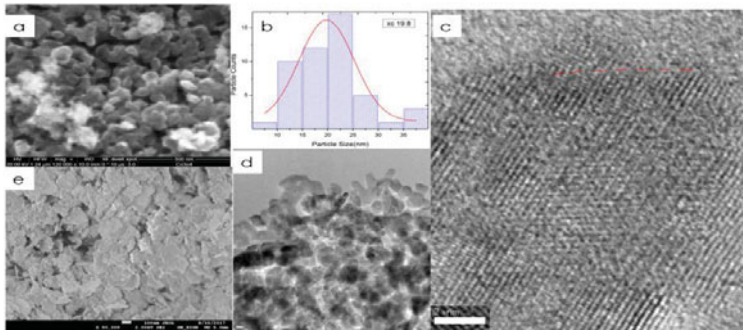

Fig. 1 (a) A SEM image of the PS type Co_3O_4 nanoparticles; (b) Size distribution of the PS type $Mn_xCo_{3-x}O_4$ CSNs; (c) A HRTEM image of the PS type $Mn_xCo_{3-x}O_4$ CSNs; (d) a TEM image of the PS type $Mn_xCo_{3-x}O_4$ CSNs; (e) a SEM image of the NP type Co_3O_4 nanoparticles.

Fig. 1 shows the SEM and TEM images of Co_3O_4 nanoparticles and Co_3O_4@$Mn_xCo_{3-x}O_4$ CSNs. Fig. 1 (a) shows an SEM image of PS type Co_3O_4 nanoparticles: we observed that our PS type Co_3O_4 nanoparticles (NPs) are pseudo-spherical and octahedron-shaped. Fig. 1 (e) shows an SEM image of NP type Co_3O_4 nanoparticles, which predominantly have a nanoplate morphology. Fig. 1 (d), which shows a TEM image of PS type $Mn_xCo_{3-x}O_4$ CSNs, indicated that there was no change in shape after manganese ions incorporated in the formation of our Co_3O_4@$Mn_xCo_{3-x}O_4$ CSNs. A histogram plot of the size distribution

of the PS type Co_3O_4@$Mn_xCo_{3-x}O_4$ CSNs is shown in Fig. 1 (b), from which we obtained an average size of 19.8 nm. Fig. 1 (c) shows a HRTEM image of the PS type CSNs, where the core and the shell regions can be easily distinguished by the interface as indicated in the image; and the shape of the isolated particle strongly support our SEM results of PS type Co_3O_4 nanoparticles which means the hydrothermal treatment doesn't change the shape of PS type Co_3O_4 nanoparticles; The approximate thickness of the shell region from the HRTEM images is ~1.3 nm. SEM-EDS and TEM-EDS results indicated the presence of manganese in the CSNs. The same crystallographic symmetry and atomic plane continuity from core to shell, due to epitaxial growth of the shell over the core, of the CSNs is seen from our TEM results.

X-ray Diffraction Analysis

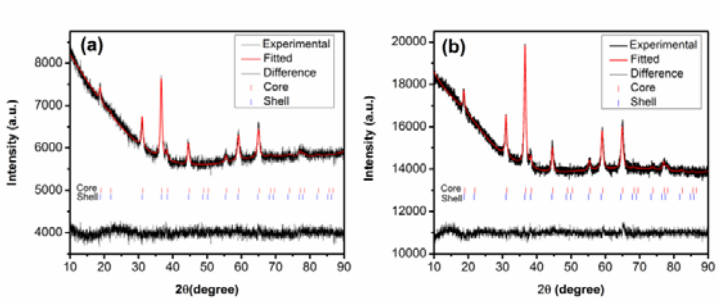

Fig. 2 XRD patterns of $Mn_xCo_{3-x}O_4$ CSNs: (a) PS type $Mn_xCo_{3-x}O_4$ CSNs; (b) NP type $Mn_xCo_{3-x}O_4$ CSNs

Fig. 2 shows that the X-ray diffraction patterns of both morphologies of $Mn_xCo_3O_4$ CSNs measured at room temperature. It is conspicuous that both of the morphologies of nanoparticles maintain the same spinel structure. This is evident from the analysis of XRD patterns measured from Co_3O_4 NPs and Co_3O_4@$Mn_xCo_{3-x}O_4$ CSNs, which yielded structures having the same $F\bar{4}3m$ symmetry for all NPs and CSNs of the study. Furthermore, we do not find any evidence for impurity phases (e.g., MnO) in the nanoparticles from the XRD data. Since the difference of the ionic radii between Mn^{2+} and Co^{2+} is small[15], Mn^{2+} ions can easily replace Co^{2+} ions with minimal distortion of the spinel crystal structure of Co_3O_4. The average crystallite size of PS Co_3O_4 nanoparticles calculated using Scherrer equation was found to be 17.30(2) nm whereas the size of PS type Co_3O_4@$Mn_xCo_{3-x}O_4$ CSNs determined by using the same method was found to be 19.40(3) nm. The latter result is consistent with the results of particle size distribution calculated from our TEM images. Thus, the growth in nanoparticles shows that Mn incorporation in the shell region with a thickness of 1.1-1.3 nm. Conversely, for the NP type CSNs, our preliminary result showed that the average crystallite size for the NP type Co_3O_4 nanoparticles is 13.2(4) nm and for the NP type CSNs the size is 21.4(2) nm, as obtained using the Scherrer equation in the analysis of XRD data. In order to further evaluate the structural properties of CSNs, Rietveld refinement was made of the XRD data. The space group symmetry of $F\bar{4}3m$ structure was used with the starting parameters for the Co^{2+} ions at the unit cell positions x = ¼, y = ¼ and z = ¼. A second $F\bar{4}3m$ CIF file was added in order to account for the shell region in the refinement. Our fitting results show consistently that the goodness-of-fit is improved significantly by use of a core-shell structure model as opposed to a single structure model. The lattice parameters of core region and shell region were found to be 8.08(0.4) Å and 8.12(2) Å for the PS type CSNs, respectively; this slight expansion of the lattice parameter is

consistent with the Shannon ionic radius of the high spin Mn^{2+} ion (0.66 Å) being slightly larger than that of high-spin Co^{2+} ion (0.58 Å) and the former partially substituting for the latter in the tetrahedral sites of the spinel structure in the shell region of the PS type CSNs. Quantitative analysis of our high resolution XPS Mn 2p3/2, Co 2p 3/2 and O 1s peaks (see reference 3 for further details on the procedures) yields a concentration of 5.31 Mn at% in the shell region of the PS type $Mn_xCo_{3-x}O_4$ CSNs. Thus, from stoichiometry calculations we estimate a chemical formula for the PS type to be $NiO@Mn_{0.84}Co_{2.16}O_{3.92}$ CSNs.

SQUID Magnetometry Measurements

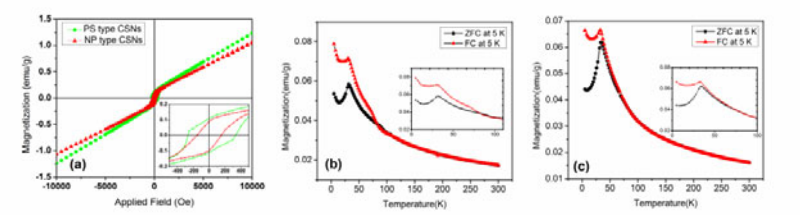

Fig. 3: Magnetometry data measured from our PS type and NP type $Co_3O_4@Mn_xCo_{3-x}O_4$ CSNs (a) FC hysteresis loops measured from PS type and NP type CSNs at 5 K; the inset shows an enlarged views of the M vs H data; (b) and (c) FC and ZFC magnetization vs. temperature data of PS type and NP type CSNs, respectively; the insets show an enlarged views of M vs. T data. The FC and ZFC data were measured at an applied field of 300 Oe. The FC hysteresis measurements were made with the samples cooled from 300 K to 5 K at 20,000 Oe.

Fig. 3 shows magnetic measurement data of PS type and NP type $Co_3O_4@Mn_xCo_{3-x}O_4$ CSNs. Fig. 3 (a) shows the field cooled (FC) hysteresis loops measure from PS type and NP type $Co_3O_4@Mn_xCo_{3-x}O_4$ CSNs at 5 K whereas the inset shows an enlarged view of the M vs H data measured at 5 K. The coercivity shown in the FC hysteresis loop for the PS type $Co_3O_4@Mn_xCo_{3-x}O_4$ CSNs is ~300 Oe whereas the coercivity for the NP type $Co_3O_4@Mn_xCo_{3-x}O_4$ CSNs is ~150 Oe, In addition to the greater coercivity, the data displayed in Fig. 3 (a) show that the PS type CSNs exhibit a much less drastic change in slope of the magnetization upon reversal from H field, either from + to – values or from – to + field, than do the NP type CSNs. The FC magnetization saturation values for the PS type and NP type CSNs at 5 K is approximately 0.11 emu/g and 0.095 emu/g, respectively. The FC vs zero field cooled (ZFC) hysteresis loops do not show significant shifts either in the negative and positive H axis directions. The exchange bias was calculated based on the formula $H_e = (H_{ZFC+} - H_{FC+} - H_{FC-} + H_{ZFC-})/2$ where the +/- indicate positive/negative H values when M=0. The exchange bias for PS type CSNs was ~33 Oe whereas for the NP type CSNs it was 6 Oe, as measured at 5 K. Our magnetometry data shows that our Co_3O_4 nanoparticles and the core regions are antiferromagnetic, whereas the incorporated Mn-substituted Co_3O_4 ($Mn_xCo_{3-x}O_4$) spinel phase of the shell region is ferrimagnetic. Thus, our CSNs have the inverted core-shell magnetic configuration. Fig.3 (b) and (c) show FC and ZFC magnetization vs temperature data measured from our PS type and NP type CSNs in the range from 5 to 300 K, respectively. These data show a spin order-disorder transition at ~33 K and a superparamagnetic blocking temperature of ~90 K for both types of CSNs. The spin order-disorder transition peaked feature appears to be more prominent in the magnetization vs temperature data of the NP type CSNs than that of the PS type CSNs.

CONCLUSIONS

We have successfully synthesized two different morphologies of Co_3O_4@$Mn_xCo_{3-x}O_4$ CSNs by using a two-step synthesis process, the first involving a soft chemical approach and the second our HNE method to develop the core-shell nanostructure. By adjustment of the pH value in the first step of the synthesis, we were able to grow CSNs having either a pseudo-spherical and octahedron-like shapes (PS) or nanoplate morphology (NP). Our characterization results confirmed that manganese ions were incorporated into the shell region of both the PS type and NP type CSNs. Our TEM results explicitly show that both two different morphologies have an explicitly have the core-shell structure and epitaxial registry of shell layers on core atomic layers. The XRD results confirm that both the core region and shell region of PS type and NP type CSNs have the spinel structure with $F\bar{4}3m$ symmetry. Our SQUID magnetometry data confirm that our CSNs have the inverted magnetic configuration with an AFM core and FiM shell.

ACKNOWLEDGEMENTS

I would like to thank Missouri State University Graduate College for a thesis funding award.

REFERENCES

1 V. Cabuil, V. Dupuis, D. Talbot, and S. Neveu, J. Magn. Magn. Mater. **323**, 1238 (2011).
2 W. Schmidt, ChemCatChem **1**, 53 (2009).
3 M.D. Hossain, R.A. Mayanovic, R. Sakidja, M. Benamara, and R. Wirth, Nanoscale **10**, 2138 (2018).
4 X.W. Lou, D. Deng, J.Y. Lee, and L.A. Archer, J. Mater. Chem. **18**, 4397 (2008).
5 X. Wang, W. Tian, T. Zhai, C. Zhi, Y. Bando, and D. Golberg, J. Mater. Chem. **22**, 23310 (2012).
6 W.Y. Li, L.N. Xu, and J. Chen, Adv. Funct. Mater. **15**, 851 (2005).
7 X. Xie, Y. Li, Z.-Q. Liu, M. Haruta, and W. Shen, Nature **458**, 746 (2009).
8 W.L. Roth, J. Phys. **25**, 507 (1964).
9 S. Fan, W. Wang, H. Ke, J.-C. Rao, and Y. Zhou, RSC Adv. **6**, 97055 (2016).
10 Y.H. Chen, J.F. Zhou, D. Mullarkey, R. O'Connell, W. Schmitt, M. Venkatesan, M. Coey, and H.Z. Zhang, AIP Adv. **5**, 087122 (2015).
11 Y. Teng, L.X. Song, L.B. Wang, and J. Xia, J. Phys. Chem. C **118**, 4767 (2014).
12 M.D. Hossain, S. Dey, R.A. Mayanovic, and M. Benamara, MRS Adv. **1**, 2387 (2016).
13 S. Dey, M.D. Hossain, R.A. Mayanovic, R. Wirth, and R.A. Gordon, J. Mater. Sci. **52**, 2066 (2017).
14 T. Athar, A. Hakeem, N. Topnani, and A. Hashmi, Int. Sch. Res. Not. (2012).
15 R.D. Shannon, Acta Crystallogr. A **32**, 751 (1976).